Discovery of reversible monoacylglycerol lipase inhibitors

Jiang, M.

Chapter 5

LEI-515 is an orally available and peripherally restricted MAGL inhibitor

M. Jiang, T. van der Wel, F. Stevens, X. Di, P. M. Gomezbarila, J. P. Medema, J. Benz, U. Grether, B.F. Florea, R. van den Berg, C. A. A. van Boeckel, M. van der Stelt*; *manuscript in preparation*.

5.1 Introduction

Monoacylglycerol lipase (MAGL) is a 33 kDa serine hydrolase that catalyzes the hydrolysis of monoacylglycerols to corresponding fatty acids and glycerol[1, 2]. Although MAGL is expressed throughout the body in various organs, such as liver, lung, testis and adipose tissue,[3] most of the current interest in the target has emerged from the finding that it is responsible for the bulk (~85%) of the metabolism of the signaling lipid 2-arachidonoyl glycerol (2-AG) in the brain[4]. 2-AG is an endocannabinoid and behaves as a full agonist for the cannabinoid CB1 and CB2 receptors.[5-7] 2-AG plays important roles in the regulation of many physiological processes, such as neuro-inflammation[8], food intake[9], pain and addiction[10]. It was also demonstrated that disrupting MAGL activity significantly reduced the levels of arachidonic acid (AA) and downstream AA-derived eicosanoids in the brain. Therefore, inhibition of MAGL could

have several therapeutic applications, like neuroprotection, anti-neuroinflammation and antinociception. [11] To date, most reported MAGL inhibitors have been designed to target the central nervous system (CNS) (See Chapter 1).[12-15]

Of note, MAGL blockade exerted also protective effects in lung and liver injury models through enhancing endocannabinoid and lowering eicosanoid levels.[16, 17] Since MAGL only controls eicosanoid metabolism in specific tissues such as the brain, liver and lung, but not in the gut[18], MAGL inhibitors might avoid some of the mechanism-based gastrointestinal and cardiovascular side effects observed with dual cyclooxygenase 1/2 (COX1/2) and selective COX2 inhibitors[19]. It is suggested that MAGL inhibitors may even protect against COX inhibitor-induced gastrointestinal injury via endocannabinoid-dependent mechanisms.[18, 20] Moreover, pharmacological and genetical inhibition of MAGL reduced tumor growth in ovarian, melanoma and prostate xenograft models.[21, 22] Therefore, development of selective peripherally restricted MAGL inhibitor may be of great value for the treatment of inflammatory and cancer.

In this chapter, **LEI-515** (Figure 1), which was identified in chapter 4 as a subnanomolar potent MAGL inhibitor with a pKi of 9.4, is further profiled in biochemical, cellular and ADME-T assays as well as mouse pharmacokinetic and target engagement studies to assess its ability to act as a reversible and in vivo active MAGL inhibitor.

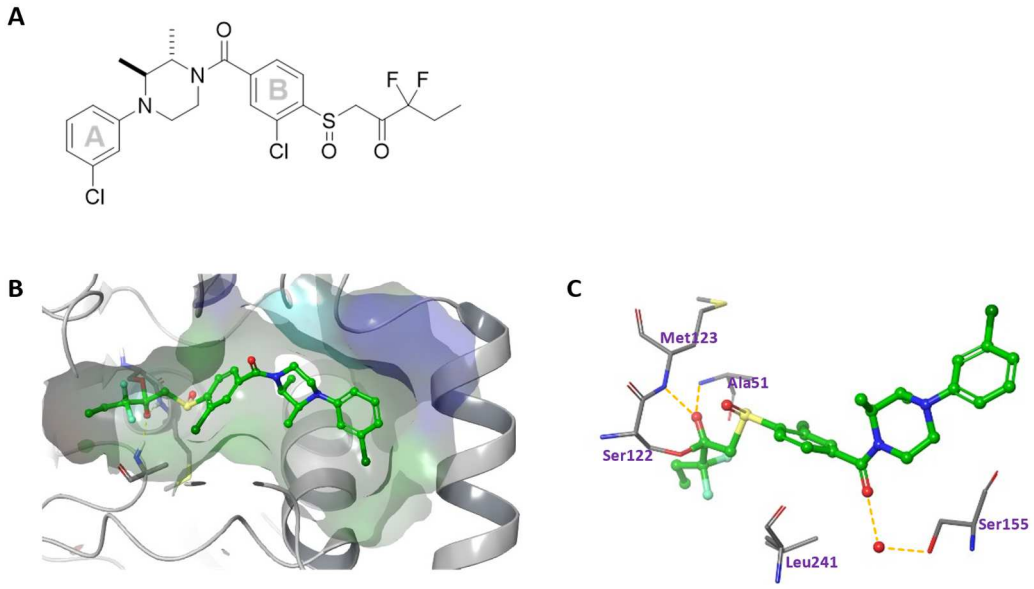

Figure 1. (A) Chemical structure of **LEI-515**. (B**,** C) X-ray cocrystal structure of **LEI-515** bound to hMAGL.

5.2 Results

LEI-515 is thought to inhibit MAGL via forming a covalent, though reversible, enzyme-inhibitor hemiketal adduct. To investigate this hypothesis, co-crystallization studies were performed using human recombinant MAGL[23] and racemic **LEI-515**. The X-ray structure of one isomer of **LEI-515** (1-((2-Chloro-4-((*2S*,*3S*)-4-(3-chlorophenyl)-2,3-dimethylpiperazine-1-carbonyl)phenyl)sulfinyl)-3,3-difluoropentan-2-one) bound to MAGL was obtained and solved at 1.55 Å resolution (Figure B and C). **LEI-515** was found to covalently attach to the catalytic Ser122 residue through its electrophilic carbonyl group as a deprotonated hemiketal. The negative charge was stabilized by two hydrogen bounds (yellow dotted lines, Figure 3C) with Ala51 and Met123, respectively. The terminal ethyl group inserted into the hydrophilic cytoplasmic access (CA) channel, while the rest of the compound occupies the large hydrophobic tunnel and the terminal chlorophenyl ring (ring A) orientated to the lid domain. The chloro group on ring B occupied a hydrophobic subpocket and the two methyl groups on the piperazine ring adopt a di-axial conformation, which enhance the hydrophobic interaction. The carbonyl of the amide group formed a water-mediated hydrogen bond with the side chain of Ser155.

Next, the selectivity of **LEI-515** over a panel of serine hydrolases was assessed by using activity-based protein profiling (ABPP), which has emerged as a powerful chemical biological technique to assess inhibitor activity and selectivity in complex and native proteomes.[24, 25] It makes use of activity-based probes (ABPs) to assess the functional state of entire enzyme classes directly in biological systems. Fluorophosphonates (FPs) and β-lactones are used as ABPs targeting serine hydrolases.[26, 27] ABPs with fluorescent reporter groups enable visualization of enzyme activities in complex proteomes by SDS–polyacrylamide gel electrophoresis (SDS-PAGE) and in-gel fluorescence scanning, while ABPs with a biotin reporter group enable affinity enrichment and identification of enzyme activities by mass spectrometry (MS)-based proteomics.[26] As shown in Figure 2A, **LEI-515** reduced MAGL activity in a dose-dependent manner with a half maximal inhibitory concentration (IC_{50}) of 25 nM in mouse brain proteome and displayed >500-fold selectivity over diacylglycerol lipase (DAGL-α) and α/β-hydrolase domain containing 6 and 12 (ABHD6 and 12), which are enzymes involved in 2-AG biosynthesis and degradation, respectively. Moreover, **LEI-515** did not inhibit fatty acid amide hydrolase (FAAH), which degrades the other endocannabinoid anandamide. Mass spectrometry (MS)-based chemical proteomics using MB108 and FP-biotin confirmed the gel-based ABPP findings[28]. **LEI-515** did not reduce labeling of the detected proteins by more than 50%, except for MAGL and identified only hormone sensitive lipase (LIPE) as a potential off-target in lung, liver and brain (Figure 2B). Next, **LEI-515** was profiled for general off-target pharmacology in a binding/functional panel comprising a panel of 44 enzymes, transporters, receptors, and ion channel targets (CEREP). **LEI-515** showed >100-fold selectivity over those ion channels, receptors and enzymes, including the cannabinoid receptors (CB1R and CB2R), hERG channel and cyclooxygenases (COX1 and COX2) (Table S1).

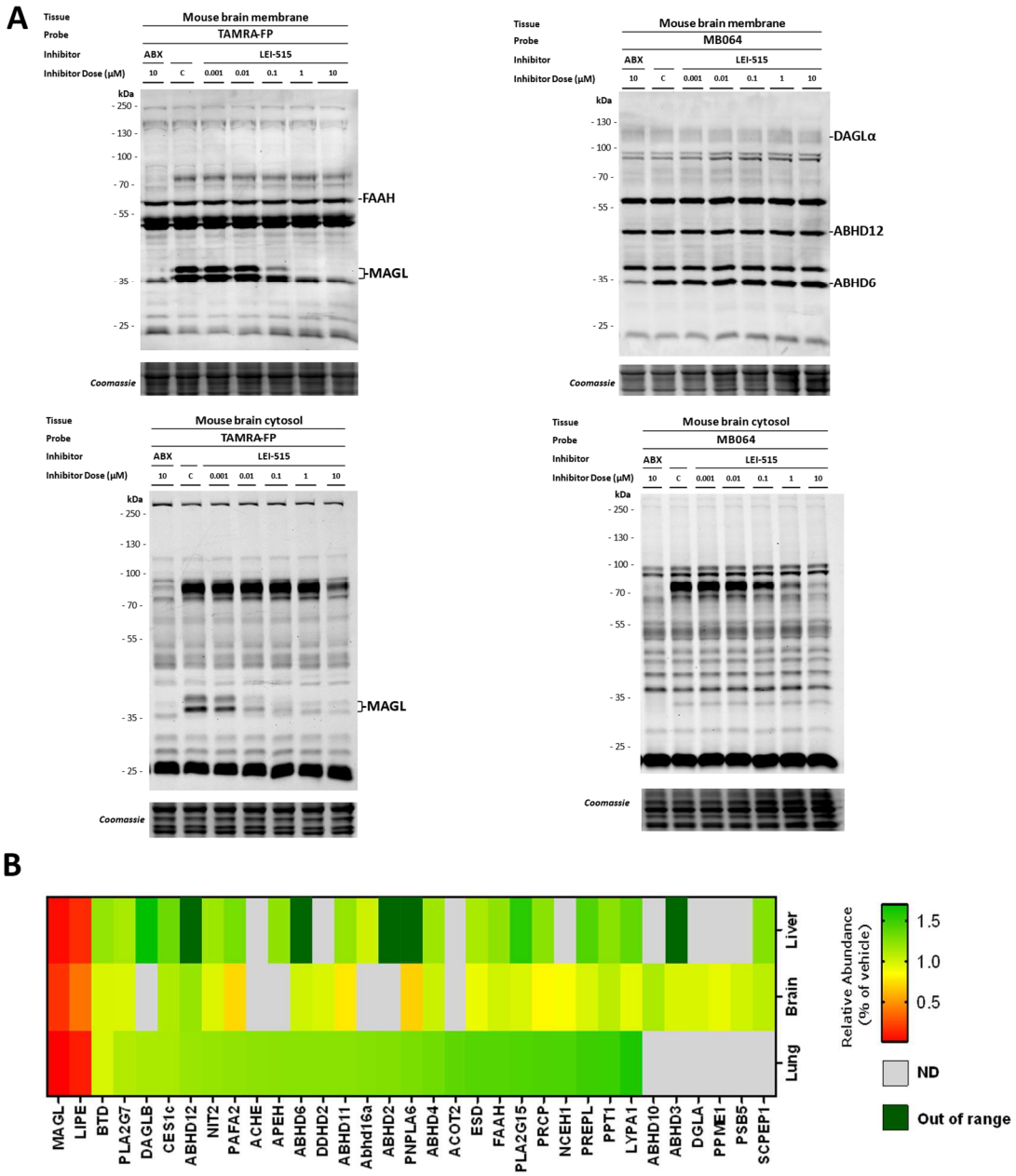

Figure 2. Selectivity profiling of **LEI-515**. (A) Competitive ABPP with **LEI-515** in mouse brain proteome using broad-spectrum probes TAMRA-FP (100 nM, 10 min) and MB064 (250 nM, 10 min). (B) Selectivity profiles of **LEI-515** on mouse brain, lung and liver proteomes using broad-spectrum probes MB108 and FP-biotin (10µM, 60min) for chemical proteomics (N = 4).

To determine the mode-of-action (covalent reversible versus irreversible) of **LEI-515**, mouse brain membrane proteome was pre-incubated with **LEI-515** or the irreversible MAGL inhibitor ABX-1431 at the IC_{80} concentration and the remaining MAGL activity was visualized with an irreversible MAGL-specific probe LEI-463[29] in a time-dependent manner. No recovery of MAGL activity was found for ABX-1431,

whereas MAGL activity was regained after approximately 40 min with **LEI-515** (Figure 3A and B). This indicated that **LEI-515** is a reversible MAGL inhibitor.

Having established that LEI-515 is a selective covalent, reversible MAGL inhibitor, we then investigated whether **LEI-515** inhibits endogenous MAGL in living cells. To this end, a panel of human breast cancer cell lines was screened with MAGL-specific probe for endogenous MAGL activity, in which four cell lines (UACC893, MDA-MB-415, HS578t and MDA-MB-435s) were found to express high level of MAGL protein and activity (Figure S1). HS578t was selected as a representative example for cellular target engagement studies using targeted lipidomics. The cells were incubated with **LEI-515** and the cellular 2-AG and AA levels were determined with liquid chromatography–mass spectrometry/mass spectrometry (LC-MS/MS). **LEI-515** increased 2-AG levels in a time-dependent manner and the cellular 2-AG level reached a plateau (around 2000 fmol/mg) after 1 h inhibitor incubation (Figure 3C). Treatment of intact HS578t cells with **LEI-515** following an 1 h inhibitor incubation time caused concentration dependent inhibition of MAGL activity with an IC_{50} value between 300 nM and 1 μM (Figure 3D), which is over 600-fold less potent than that observed in the biochemical assay (Chapter 4, Table 3). One potential explanation for the gap is that the local 2-AG concentration in the intact cells is higher than in the biochemical assay. In addition, **LEI-515** also decreased the cellular level of AA and anandamide (AEA) (Figure 3E). It is normal to see a reduction of AA level as AA is the product of 2-AG hydrolysis and the decreased AA level might cause the reduction of AEA level.

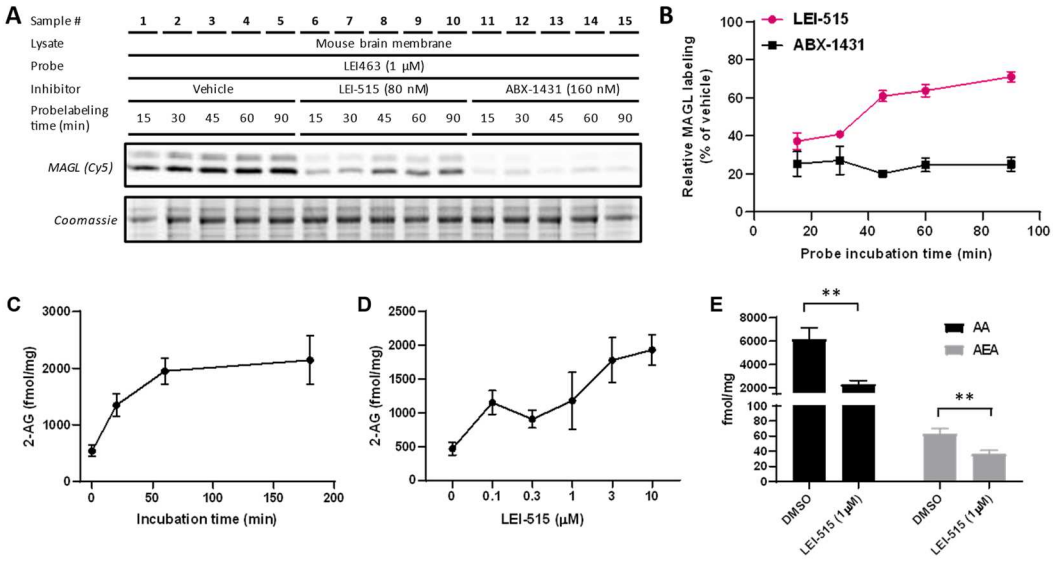

Figure 3. Reversibility profiling of **LEI-515**. (A, B) Time-dependent recovery of MAGL activity as determined by using competitive ABPP with MAGL selective probe LEI-463. Mouse brain proteome (2 mg/ml) was preincubated with **LEI-515** (10 min) or ABX-1431 (15 min). (C) *In situ* treatment of HS578t cells with **LEI-515** (1 µM) time-dependently increased cellular 2-AG levels (N = 5). (D) *In situ* treatment of HS578t cells with **LEI-515** (1 h) dose-dependently increased cellular 2-AG levels (N = 4). (E) *In situ* treatment of HS578t cells with **LEI-515** (1 µM, 1 h) decreased cellular AA and AEA levels. Statistical analysis: one-way ANOVA (*** = $p < 0.001$, ** = $p < 0.01$, * = $p < 0.05$ vs vehicle).

Inhibition of MAGL has been shown to suppress tumorigenesis and progression in a number of cancer cell lines, including colorectal cancer cells.[30, 31] To investigate whether **LEI-515** inhibits cancer cell growth, a cell viability assay was performed. Eighteen colorectal cancer cell lines were incubated with **LEI-515** for 72 h in delipidated medium and the cell viability was determined. **LEI-515** impaired those colorectal cancer cells growth with concentration for 50% of maximal effect (EC_{50}) in the range from 2 to 20 µM, except for MDST8, LS1031 and Snu-c1 cell lines (Figure 4). The EC_{50} values were plotted against MAGL mRNA levels in the colorectal cancer cell lines and no correlation was found. Actually, **LEI-515** showed higher EC_{50} on the cell lines with lower MAGL mRNA level (Figure S2). This might due to off-target effects of **LEI-515**, such as the inhibition of LipE. It would be interesting to also determine the MAGL and LipE protein levels with western blot and MAGL activity levels with ABPP in those cell lines.

Before testing whether **LEI-515** possesses *in vivo* efficacy, the absorption,

distribution, metabolism and excretion (ADME) profile of **LEI-515** was determined. **LEI-515** demonstrates acceptable physicochemical properties for oral bioavailability (MW = 531 Da, cLogP = 4.7 and topological polar surface area (tPSA) = 58 $Å^2$). **LEI-515** shows high stability (100 % remaining after 180 min) in both human and mouse plasma. Clearance in human microsomes (30.9 µL/min/mg) is moderate and low in mouse microsomes (< 3.4 µL/min/mg). **LEI-515** exhibits high human and mouse protein binding (99.6% for both). **LEI-515** shows negligible cell permeability in Caco-2 cells (P_{app}A-B < 0.01 × 10^{-6} cm/s and P_{app}B-A < 0.005 × 10^{-6} cm/s). This might due to the specific binding of **LEI-515** with endogenous MAGL in Caco cells or transporter proteins which efflux **LEI-515** out of the cells. Pharmacokinetic analysis (DMSO/Kolliphore/5% mannitol in water (1/1/8, v/v) was used as vehicle) (Figure 5) for **LEI-515** in male C57BL/6J mice reveals a moderate clearance (CL = 35 mL/min/kg) and volume of distribution (V_{ss} = 2.1 L/kg), resulting in a half-life of 4.5 h. In the same species **LEI-515** shows excellent bioavailability after oral administration (F_{po} = 81 %) and quick absorption (T_{max} = 0.5 h). These results are contradictory with the result from Caco-2 assay. A possible explanation is that the compound was directly absorbed through the stomach. Most interestingly, the brain to plasma ratio was 0.01 at maximum serum concentration (C_{max}), which demonstrates that **LEI-515** is a peripherally restricted MAGL inhibitor.

A

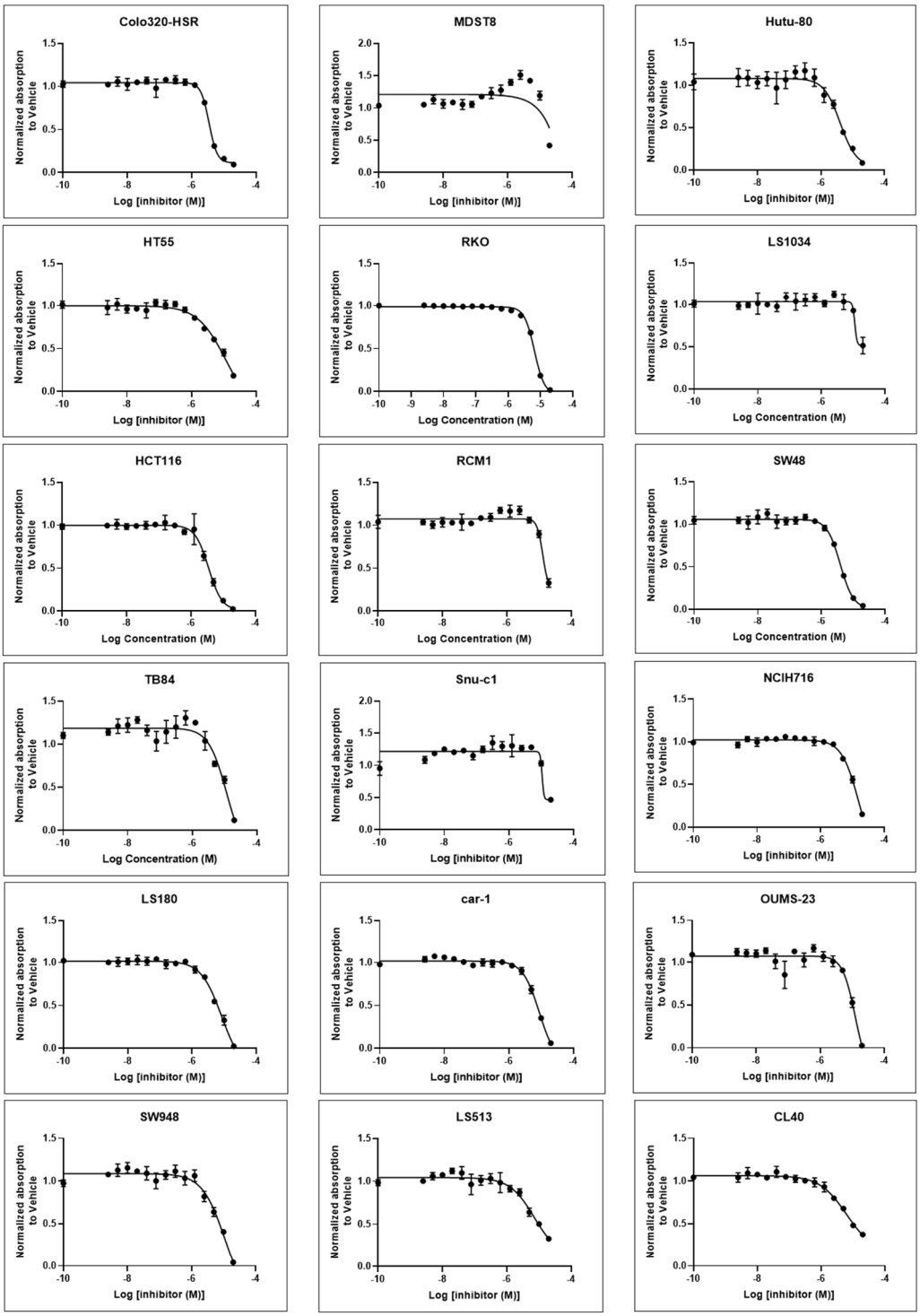

B

Cell line	pEC_{50}	Cell line	pEC_{50}	Cell line	pEC_{50}
Colo320-HSR	5.5 ± 0.1	HCT116	5.5 ± 0.1	Hutu-80	5.4 ± 0.1
SW48	5.4 ± 0.1	RKO	5.2 ± 0.1	CL40	5.2 ± 0.1
LS180	5.1 ± 0.1	car-1	5.1 ± 0.1	LS513	5.1 ± 0.1
RCM1	4.9 ± 0.3	HT55	4.9 ± 0.2	TB84	4.9 ± 0.2
OUMS-23	4.9 ± 0.1	SW948	4.9 ± 0.1	NCIH716	4.8 ± 0.1
MDST8	< 4.7	LS1034	< 4.7	Snu-c1	< 4.7

Figure 4. Anti-cancer effects of **LEI-515** on 18 colorectal cancer cell lines (n = 3).

In view of the encouraging PK properties, *in vivo* target engagement experiments were performed. Male C57/6J mice were treated with LEI-515 (3 and 10 mg/kg, p.o.) or vehicle (DMSO/Kolliphore/5% mannitol in water (1/1/8, v/v)) and then sacrificed after 1h to determine whether 2-AG levels were elevated. To this end, lipid levels as well as **LEI-515** concentration in the brain and lung were analyzed by LC-MS. **LEI-515** appeared to increase 2-AG levels and decrease AA levels in the lung at 10 mg/kg. However, the difference is not statistically significant (Figure 6A). The lack of effect might be due to the high protein binding of the compound, which may have reduced the available free fraction of **LEI-515**, or insufficient exposure time. Of note, a correlation ($R^2 = 0.7$, $q < 0.001$) between LEI-515 concentration and 2-AG levels in the lung was observed (Figure S3). No significant change of the 2-AG, AA and eicosanoids levels in the brain was observed after treatment of **LEI-515** (Figure 6B and Figure S3), which is in agreement with the reduced brain penetration.

A

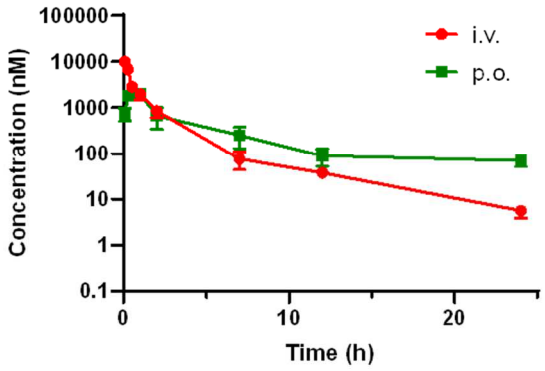

B

	p.o.	i.v.
Dose (mg/kg)	10	10
CL (ml/min/kg)	-	35
$\mathbf{V_{ss}}$ (L/kg)	-	2.1
$\mathbf{t_{1/2}}$ (h)	-	4.5
$\mathbf{C_{max}}$ (nM)	2433	-
$\mathbf{t_{max}}$ (h)	0.5	-
AUC (h.nmol/L)	7330	-
$\mathbf{F_{po}}$ (%)	81	-
$\mathbf{C_{brain}/C_{plasma}}$	0.01	-

Figure 5. Pharmacokinetics (PK) profile of **LEI-515** in C57BL/6J mice. (A) *In vivo* PK of **LEI-515** in plasma of mice via intravenous (i.v., 10 mg/kg) or oral (p.o., 10 mg/kg) administration. (B) PK parameters of **LEI-515** in mice after p.o. and i.v. administration. **CL** = clearance. $\mathbf{V_{ss}}$ = volume of distribution at steady state. $\mathbf{t_{1/2}}$ = half life. $\mathbf{C_{max}}$ = maximum plasma drug concentration. $\mathbf{t_{max}}$ = time to reach C_{max}. **AUC** = area under plasma concentration time curve. **F** = bioavailability.

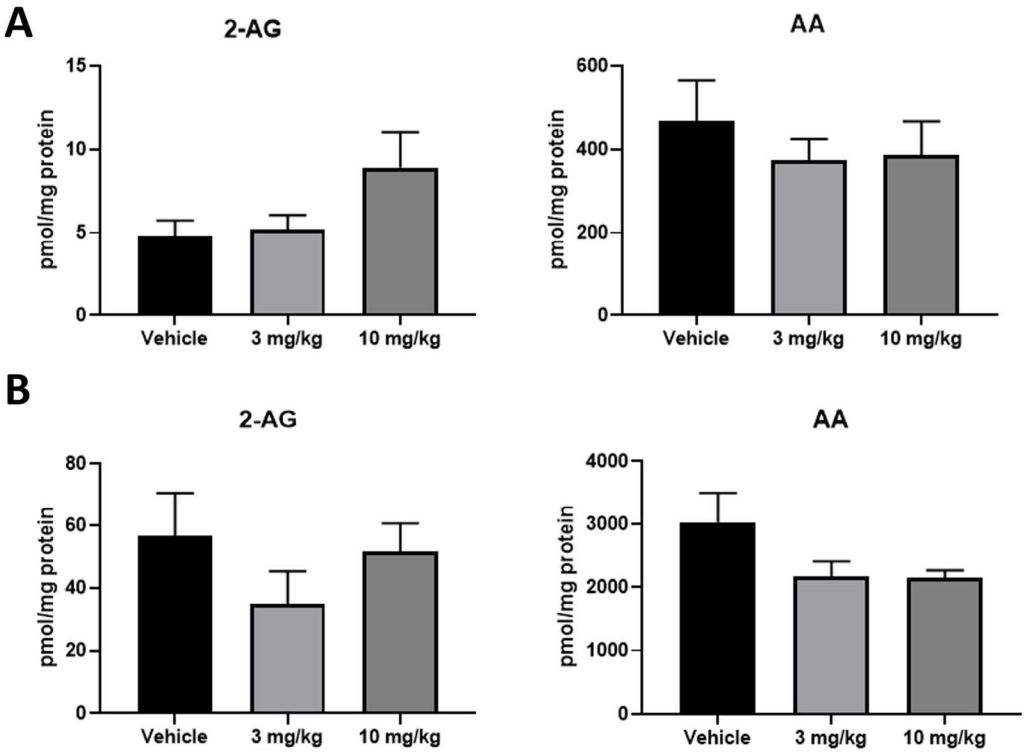

Figure 6. *In vivo* target engagement of **LEI-515** in C57BL/6J mice. (A) Absolute lipid levels of 2-AG and AA in the lung (n = 5). (B) Absolute lipid levels of 2-AG and AA in the brain (n = 5).

5.3 Conclusion

In conclusion, crystallography studies showed that LEI-515 bound to MAGL covalently and only one isomer of **LEI-515** (1-((2-Chloro-4-((*2S*,*3S*)-4-(3-chlorophenyl)-2,3-dimethylpiperazine-1-carbonyl)phenyl)sulfinyl)-3,3-difluoropentan-2-one) was observed in the binding pocket. Comparative and competitive chemical proteomics using broad-spectrum probes (MB-064 and TAMRA-FP) in combination with MAGL-specific probe LEI-463 was applied to characterize the MAGL inhibitor **LEI-515**. This inhibitor was found to be a reversible MAGL inhibitor with high selectivity against a panel of serine hydrolases, enzymes, receptors and ion channels. Targeted lipidomics revealed that **LEI-515** is able to increase 2-AG levels in a time- and concentration-dependent manner in human breast cancer cells and could inhibit cell proliferation in an array of colon cancer cell lines. Pharmacokinetics studies demonstrated that **LEI-515** is an orally available and peripherally restricted MAGL inhibitor. According to our

knowledge, **LEI-515** is the first and most selective peripherally restricted MAGL inhibitor to date**. LEI-515** showed low *in vivo* efficacy, which might due to the high protein binding or insufficient exposure time. For future investigation, the *in vivo* target engagement experiment should be repeated with higher dosing (such as 30 mg/kg) or longer exposure time (such as 2 h.). It would also be interesting to study **LEI-515** in various animal models of human diseases, such as hepatic ischemia/reperfusion (I/R), lung I/R and cancer. Taken together, **LEI-515** could be a useful compound to study MAGL function in peripheral tissues without disturbing the MAGL activity in the CNS or further developed as drug candidate with limited central side effects.

5.4 Experimental procedures

Crystallization studies. Human MAGL protein with mutations introduced at positions Lys36Ala, Leu169Ser and Leu176Ser[23] was concentrated to 10.8 mg/ml. Crystallization trials were performed in sitting drop vapor diffusion setups at 21 °C. Crystals appeared within 2 days out of 0.1M MES pH 6.5, 6 to 13% PEG MME5K, 12% isopropanol. Crystals were soaked in crystallization solution supplemented with 10 mM LEI-515 for 16 hours.

For data collection crystals were flash cooled at 100 K with 20 % ethylene glycol added as cryo- protectant. X-ray diffraction data were collected at a wavelength of 1.00009 Å using an Eiger2X 16M detector at the beamline X10SA of the Swiss Light Source (Villigen, Switzerland). Data have been processed with XDS[32] and scaled with SADABS (BRUKER). The crystals belong to space group $C222_1$ with cell axes of a= 91.62 Å, b= 127.57 Å, c= 60.36 Å with β=90.57° and diffract to a resolution of 1.55Å. The structure was determined by molecular replacement with PHASER[33] using the coordinates of PDB entry 3pe6[23] as search model. Difference electron density was used to place LEI-515. The structure was refined with programs from the CCP4 suite[34]. Manual rebuilding was done with COOT[35]. Data collection and refinement statistics are summarized in Table 1.

Preparation of mouse tissue proteome. Mouse tissues were isolated according to guidelines approved by the ethical committee of Leiden University. Isolated tissues were thawed on ice, dounce homogenized in lysis buffer A (20 mM HEPES, 2 mM DTT, 1 mM $MgCl_2$, 25 u/ml Benzonase, pH 7.2) and incubated for 15 min on ice. Then debris was removed by low-speed spin (2500 g, 1 min, 4 °C) and the supernatant was subjected to ultracentrifugation (100.000 g, 45 min, 4 °C, Beckman Coulter, Type Ti70 rotor) to yielded the membrane fraction as a pellet and the cytosolic fraction in the supernatant. The membrane fraction was resuspended in lysis buffer B (20 mM HEPES, 2 mM DTT). The total protein concentration was determined with Quick Start Bradford assay. The obtained membranes and supernatant were flash frozen in liquid nitrogen and stored in small aliquots at -80 °C until use.

Activity based protein profiling on mouse brain proteome. The competitive ABPP assay on mouse brain proteome was performed as previously reported.[36] In brief, to 19 µl mouse brain proteome (2mg/ml) was added 0.5 µl of the inhibitor or pure DMSO, vortexed gently and incubated for 30 min at RT. Subsequently, 0.5 µl probe was added to the proteome sample, vortexed gently and incubated for 10 min. The reaction was quenched by adding 10 µl of 4*Laemmli-buffer and 10 µl of quenched reaction mixture was resolved on 10 % acrylamide SDS-PAGE (180V, 75 min). Fluorescence was measured using a Biorad ChemiDoc MP system. Gels were then stained using Coomassie staining and imaged for protein loading control.

Table 1: Data collection and refinement statistics for human MAGL LEI-515 complex.

	hMAGL-**LEI-515** complex
Data collection	
Space group	$C222_1$
Cell dimensions	
a, *b*, *c* (Å)	91.62, 127.57, 60.36
α, β, γ (°)	90, 90, 90
Resolution (Å)	1.55 (1.65-1.55)
R_{sym} or R_{merge}	0.059 (0.78)
$I / \sigma I$	11.69 (1.13)
Completeness (%)	99.6 (99.4)
Redundancy	6.62 (6.16)
Refinement	
Resolution (Å)	48.3 – 1.55
No. reflections	48898
R_{work} / R_{free}	15.43/18.03
No. atoms	
Protein	2299
Water	325
Ligand	34
B-factors	
Protein	25.56
Water	47.53
Ligand	33.07
R.m.s. deviations	
Bond lengths (Å)	0.016
Bond angles (°)	1.999

*Values in parentheses are for highest-resolution shell.

Chemical proteomics. Activity-based proteomics was performed based on previously described procedures. [37] Mouse tissue proteome (245 µL, 2.0 mg/mL) membrane or soluble fraction was incubated with vehicle (DMSO) or inhibitor (1 µM) in DMSO for 30 minutes at 37 ºC. The proteome was labeled with a probe cocktail (2.5 µM MB108 and 5 µM FP-Biotin, 30 minutes, 37 ºC). Subsequently the labeling reaction was quenched and excess probe was removed by chloroform methanol precipitation. Precipitated proteome was suspended in 250 µL 6M Urea/25 mM ammonium bicarbonate and allowed to incubate overnight. 2.5 µL (1 M DTT) was added and the mixture was heated to 65 ºC for 15 minutes. The sample was allowed to cool to rt before 20 µL (0.5 M) iodoacetamide was added and the sample was alkylated for 30 minutes in the dark. 70 µL 10% (wt/vol) SDS was added and the proteome was heated for 5 minutes at 65 ºC. The sample was diluted with 6 mL PBS. 100 µL of 50% slurry of Avidin−Agarose from egg white (Sigma-Aldrich) was washed with PBS and added to the proteome sample. The beads were incubated with the proteome > 3h. The beads were isolated by centrifugation and washed with 0.5% (wt/vol) SDS and PBS (3x). The proteins were digested overnight with sequencing grade trypsin (Promega) in 250 µL OB-Dig buffer (100 mM Tris, 100 mM NaCl, 1 mM $CaCl_2$, 2 % ACN and 500 ng trypin) at 37 °C with vigorous shaking. The pH was adjusted with formic acid to pH 3 and the beads were removed and the beads were removed from filtration. The peptides were washed and eluted with stage tips according to the procedure below.

Step	Solution	Centrifugation speed
Conditioning 1	50 µL MeOH	2 min 300g
Conditioning 2	50 µL Stage tip solution B	2 min 300g
Conditioning 3	50 µL Stage tip solution A	2 min 300g
Loading		2 min 600g
Washing	100 µL Stage tip solution A	2 min 600g
Elution	100 µL Stage tip solution B	2 min 600g

Stage tip solution A: 0.5% (vol/vol) FA in H_2O. (Freshly prepared solution)

Stage tip solution B: 0.5% (vol/vol) FA in 80% (vol/vol) ACN/H_2O. (Freshly prepared solution).

After the final elution step, the obtained peptides were concentrated on a speedvac to remove the ACN. The residue was reconstituted in 95:3:0.1 H_2O/ACN/FA (vol/vol) before LC/MS analysis.

For LC-MS analysis, each sample in duplicate was loaded onto the ultra-performance liquid chromatography-ion mobility spectrometry-mass spectrometry system a NanoACQUITY UPLC System coupled to SYNAPT G2-Si high-definition mass spectrometer[37]. A trap-elute protocol was followed, where 1 µL of the digest was loaded on a trap column (C18 100 Å, 5 µM, 180 µMx20 mm; Waters), followed by elution and separation on an analytical column (HSS-T3 C18 1.8µM, 75 µMx250 mm; Waters). The sample was loaded onto this column at a flow rate of 10 µL/min with 99.5% solvent A for 2 minutes before switching to the analytical column. Peptide separation was achieved by using a multistep concave gradient based on gradients previously described[38]. The column was re-equilibrated to initial conditions after washing with 90% solvent B as previously described[38]. The rear seals of the pump were flushed every 30 minutes with 10% (v/v) acetonitrile. [Glu1] fibrinopeptide B was used as a lock mass compound. The auxiliary pump of the LC system was used to deliver this peptide to the reference sprayer (0.2 µL/min). An ultradefinition MSE method was set up as previously described[38]. Briefly, the mass range was set at 50-2,000 Da, with a scan time of 0.6 seconds in positive resolution mode. The collision energy was set to 4 V in the trap cell for low-energy MS mode. For the elevated energy scan, the transfer cell collision energy was ramped using drift-time specific collision energies. The lock mass was sampled every 30 seconds.

Targeted lipidomics

The targeted lipidomics experiments are based on previously reported methods with small alterations [26].

Cell culture. All cells were cultured at 37 ºC and 7 % CO_2 in RPMI-1640 with GlutaMax (2 mM), penicillin (100 µg/ml), streptomycin (100 µg/ml) and 10 % fetal bovine serum (Biowest).

Activity based protein profiling in breast cancer cells. The cells pellets were suspended in lysis buffer (20 mM HEPES pH7.2, 2 mM DTT, 1 mM $MgCl_2$, 25 u/ml

Benzonase) and homogenized. The protein **ABPP in human breast cancer cells.** Cell pellets were suspended in lysis buffer (20 mM HEPES pH 7.2, 2 mM DTT, 1 mM $MgCl_2$, 25 u/mL Benzonase) and homogenized. The protein concentration was determined by Quick Start Bradford assay (Biorad). The breast cancer cell proteome (2 mg/ml) was incubated with ABP LEI-463 (100 nM) for 30 min. Then the reaction was quenched with standard SDS PAGE sample buffer. Gels were scanned using a ChemiDoc MP system.

Western Blot. Proteins on SDS-PAGE gels were transferred to 0.2 µm PVDF membranes using the Trans-Blot Turbo transfer system (Bio-Rad) and blocked with blocking buffer (5% (w/v) milk in 10 mL TBS-Tween) for 1 hour. Membranes were stained with primary rabbit anti-MAGL antibody (Abcam #ab24701; 0.5% (v/v) in 2 mL blocking buffer) for 16h at 4°C. After three washing steps with TBS-Tween, goat anti-rabbit IgG-HRP antibody (Santa Cruz sc-2030; 0.02% (v/v) in 2 mL blocking buffer) was added and incubated for 1 hour at rt. The blot was washed three times with TBS-Tween and once with TBS before analysis. All washing steps were performed with 5 mL for 10 min. The western blot was visualized by discarding the TBS buffer and addition of imaging solution (10 mL luminal, 100 µL ECL enhancer, 3 µL H_2O_2) in the dark. After 5 minutes, the blot was scanned for chemiluminescence. Actin was used as a loading control. After imaging, blots were blocked as previously described and stained with primary mouse anti-Actin antibody (Abcam #ab8226; 0.1 (v/v) in 2 mL blocking buffer) for 1 hour at rt. After washing, blots were stained with secondary goat anti-mouse IgG-HRP antibody (Santa Cruz sc-2031; 0.02% (v/v) in 2 mL blocking buffer) for 1 hour at rt. After washing three times with TBS-Tween and once with TBS, blots were scanned for chemiluminescence. Images were analyzed with Image Lab 4.1.

Lipidomics Sample preparation. Here, 3×10^6 HS578t cells were seeded 1 d before treatment in 10 cm dishes. Before treatment, cells were washed twice with warm PBS and then treated with vehicle or compound in 10 ml medium without serum. Washing with cold PBS (1×) followed by gathering in 1.5 ml Eppendorf tubes and centrifugation (10 min, 1,500 r.p.m.). PBS was removed and the cell pellets were flash frozen with liquid nitrogen and stored at −80 °C. Next, 10% of each cell sample (collected during

harvesting) was used to determine the protein concentration using a Bradford assay (Bio-Rad) for normalization after lipid measurements.

Lipid extraction. Lipid extraction was performed on ice. Samples were thawed on ice and spiked with 10 µL deuterium labeled internal standard mix (Table 1), vortex and incubate for 5 minutes on ice. Subsequently 100 µL 0.5 % sodium chloride and 100 µL ammonium acetate buffer (0.1 M, pH 4) were added. After extraction with 1 mL methyl tert-butyl ether (MTBE), tubes were thoroughly mixed for 7 min using a bullet blender blue (Next advance Inc., Averill park, NY, USA) at speed 8, followed by a centrifugation step (16,000g, 11 min, 4 °C). Next, 925 µL of the upper MTBE layer was transferred into a clean 1.5 mL Safe-Lock Eppendorf tube. Samples were dried in a speedvac (Eppendorf, 45 min, 30 °C) and reconstituted in acetonitrile/water (30 µL, 90:10, v/v). The samples were thoroughly mixed for 4 min, followed by a centrifugation step (10.000g, 4 min, 4°C) and transferred to a LC-MS vial (9 mm, 1.5 mL, amber screw vial, KG 090188, Screening Devices) with insert (0.1 mL, tear drop with plastic spring, ME 060232, Screening devices). 5 µl of each sample was injected in to the LC-MS/MS system.

LC-MS/MS Analysis. A targeted analysis of 26 compounds, including endocannabinoids, related N-acylethanolamines (NAEs) and free fatty acids (Table **2**), was measured using an Acquity UPLC I class binary solvent manager pump in conjugation with a tandem quadrupole mass spectrometer as mass analyzer (Waters Corporation, Milford, USA). The separation was performed with an Acquity HSS T3 column (2.1 × 100 mm, 1.8 µm) maintained at 45 °C. The aqueous mobile phase A consisted of 2 mM ammonium formate and 10 mM formic acid, and the organic mobile phase B was acetonitrile. The flow rate was set to 0.55 mL/min; initial gradient conditions were 55 % B held for 0.5 min and linearly ramped to 60 % B over 1.5 min. Then the gradient was linearly ramped to 100 % over 5 min and held for 2 min; after 10 s the system returned to initial conditions and held 2 min before next injection. Electrospray ionization-MS and a selective Multiple Reaction Mode (sMRM) was used for endocannabinoid quantification. Individually optimized MRM transitions using their synthetic standards for target compounds and internal standards are described in

Table **2**. Peak area integration was performed with MassLynx 4.1 software (Waters Corporation). The obtained peak areas of targets were corrected by appropriate internal standards peak area. Calculated response ratios, determined as the peak area ratios of the target analyte to the respective internal standard peak area, were used to obtain absolute concentrations from their respective calibration curves.

Table 2: LC-MS Standards and deuterium labeled internal standards for lipidomics analysis. Q1 and Q3 are optimized precursor ion and product ion respectively and expressed as m/z. DP and CE are declustering potential (volt) and collision energy (Volt) respectively.

Abbreviation	Name	Q1	Q3	DP, CE	*Polarity*
1 & 2-AG (20:4)	1-Arachidonoyl Glycerol	379.21	287.2	45, 10	
1-LG (18:2)	1-Linoleoyl Glycerol	355.34	246	48, 10	
2-LG (18:2)	2-Linoleoyl Glycerol	357.34	247.5	48, 10	
2-OG (18:1)	2-Oleoyl Glycerol	357.34	247.5	40, 12	
1-OG (18:1)	1-Oleoyl Glycerol	357.34	247.5	40, 12	
AEA (20:4)	Arachidonoyl Ethanolamide	348.40	62.02	35, 16	
DEA (22:4)	Docosatetraenoyl Ethanolamide	376.38	61.92	55, 18	
DGLEA (18:3)	Dihomo-γ-Linolenoyl Ethanolamide	350.38	61.98	40, 14	+
DHEA (22:6)	Docosahexaenoyl Ethanolamide	372.38	62.01	50, 14	
EPEA (20:5)	Eicosapentaenoyl Ethanolamide	346.34	61.98	36, 16	
LEA (18:2)	Linoleoyl Ethanolamide	324.34	61.98	35, 14	
OEA (18:1)	Oleoyl Ethanolamide	326.4	62.01	45, 16	
PDEA (15:0)	Pentadecanoyl Ethanolamide	286.34	62.01	45, 12	
PEA (16:0)	Palmitoyl Ethanolamide	300.34	61.98	42, 14	
POEA (16:1)	Palmitoleoyl Ethanolamide	298.34	62.01	45, 14	
SEA (18:0)	Stearoyl Ethanolamide	328.38	61.98	45, 16	
AA (20:4)	Arachidonic Acid	302.28	259.3	-40, -12	-

PA (FA 16:0)	Palmitic Acid	255.33	237.24	-50, -20	
SA (FA 18:0)	Stearic Acid	283.34	265.31	-60, -22	
OA (FA 18:1)	Oleic Acid	281.34	263.31	-50, -20	
LA (FA 18:2)	Linoleic Acid	279.34	261.25	-64, -16	
GLA (FA 18:3)	y-Linolenic Acid	277.3	58	-60, -20	
ETA (FA 20:3. (ω−3)	11(Z).14(Z).17(Z)-Eicosatrienoic Acid	305.28	306.09	-60, -18	
DGLA (FA 20:3. (ω−6)	Dihomo-γ-Linolenic Acid (20:3)	305.28	306.03	-66, -18	
EPA (FA 20:5.(ω−3)	Eicosapentaenoic Acid	301.34	257.3	-60, -10	
DHA (FA 22:6. (ω−3)	Docosahexaenoic Acid	327.28	283.31	-60, -10	
2-AG-d8 (20:4)	2-Arachidonoyl Glycerol-d8	387.38	294.2	45, 10	
AEA-d8 (20:4)	Arachidonoyl Ethanolamide-d8	356.38	62.79	35, 16	
DHEA-d4 (22:6)	Docosahexaenoyl Ethanolamide-d4	376.38	66.01	50, 14	
LEA-d4 (18:2)	Linoleoyl Ethanolamide-d4	328.34	66.01	35, 16	+
OEA-d4 (18:1)	Oleoyl Ethanolamide-d4	330.38	66.01	45, 16	
PEA-d5 (16:0)	Palmitoyl Ethanolamide-d5	305.34	61.98	42, 16	
SEA-d3 (18:0)	Stearoyl Ethanolamide-d3	331.38	61.91	45, 16	
EPEA-d4 (20:5)	Eicosapentaenoyl Ethanolamide-d4	350.34	66.08	36, 18	
AA-d8 (20:4)	Arachidonic Acid-d8	311.34	267.30	-40, -12	-
PA (16:0)-d31	Palmitic Acid-d31	286.5	266.37	-40, -22	

Statistical analysis. Absolute values of lipid levels were corrected using the measured protein concentrations. Data were tested for significance with GraphPad v.6 using one-way analysis of variance (ANOVA) with Tukey correction for multiple

comparisons. $P < 0.05$ was considered significant.

***In situ* anti-cancer profile**

Cell culture. Eighteen CRC cell lines were kindly provided by Sanger Institute (Cambridge, UK; authenticated by STR Genotyping). Cell lines RKO, SW48, HT55, SW948, SW1463, CL-40, LS-180, CaR-1, HUTU-80 and OUMS-23 were cultured in Dulbecco's modified Eagle's medium/F-12 medium with L-glutamine, 15 mM HEPES (Thermo-Fisher Scientific, Bleiswijk, The Netherlands) with added fetal bovine serum (Lonza, Breda, The Netherlands) and penicillin and streptomycin. HCT-116, KM12, RCM-1, SNUC1, LS-513, COLO-320-HSR, MDST8 and NCI-H716 were cultured in RPMI 1640 with L-glutamine, 25 mM HEPES (Thermo-Fisher Scientific, Bleiswijk, The Netherlands) added fetal bovine serum, penicillin and streptomycin, 1% D-glucose solution plus (Sigma-Aldrich, Zwijndrecht, The Netherlands) and 100 μM sodium pyruvate (Life Technologies, Bleiswijk, The Netherlands). All cultures were maintained in humidified 37 °C 5% CO2 incubators and cells were regularly tested for mycoplasma infection

Cell viability assay. Cell lines were seeded in 100 μl delipidated medium in a 96 well cell tissue culture plate and treated in triplicate with DMSO or a titration of the drug printed using a HP D300e Digital Dispenser one day after plating (Hewlett-Packard, Palo Alto, CA, USA). CellTiter-Blue® Cell Viability Assay (cat. #G8082, Promega) was used as a read-out three days after exposure to treatment, measured on a Synergy™ HT multi-detection microplate reader (BioTek Instruments, Winooski, VT, USA). Blank signal of medium only control was deducted from all reads before normalizing all values to the average value of the DMSO treated control (= value treated replicate / average value DMSO triplicate).

***In vitro* ADME profile and *in vivo* pharmacokinetics**

Microsomal clearance. The microsomal clearance assay was performed as previously described[39]. Pooled commercially available microsome preparations from male mouse microsomes. For human, ultrapooled liver microsomes were purchased to account for the biological variance in vivo from human liver tissues. For the microsome incubations (incubation buffer 0.1 M phosphate buffer pH 7.4), 96-deep well plates were applied,

which were incubated at 37 °C on a TECAN equipped with Te-Shake shakers and a warming device. The reduced nicotinamide adenine dinucleotide phosphate regenerating system consisted of 30 mM glucose-6-phosphate disodium salt hydrate; 10 mM NADP; 30 mM $MgCl_2 \times 6H2O$ and 5 µg/µl glucose-6-phosphate dehydrogenase in 0.1 M potassium phosphate buffer pH 7.4. Incubations of LEI-401 at 1 µM in microsome incubations of 0.5 µg/µl plus cofactor reduced nicotinamide adenine dinucleotide phosphate were performed in 96-well plates at 37 °C. After 1, 3, 6, 9, 15, 25, 35 and 45 min 40 µl incubation solutions were transferred and quenched with 3:1 (v/v) acetonitrile containing internal standards. Samples were then cooled and centrifuged before analysis by LC–MS/MS. The log peak area ratios (test compound peak area/internal standard peak area) were plotted against incubation time using a linear fit. The calculated slope was used to determine the intrinsic clearance: CL_{int} (µL /min/ mg protein) = −slope (min^{-1}) × 1,000 / (protein concentration (µg/µL)).

Plasma protein binding. The plasma protein binding assay was performed as previously described[39]. Pooled and frozen plasma from human and mouse were obtained from BioreclamationIVT. The Teflon equilibrium dialysis plate (96-well, 150 µl, half-cell capacity) and cellulose membranes (12–14 kDa molecular weight cut-off) were purchased from HT-Dialysis (Gales Ferry). Both biological matrix and phosphate buffer pH were adjusted to 7.4 on the day of the experiment. The determination of unbound compound was performed using a 96-well format equilibrium dialysis device with a molecular weight cut-off membrane of 12 – 14 kDa. The equilibrium dialysis device itself was made of Teflon to minimize nonspecific binding of the test substance. Compound were tested with an initial total concentration of 1,000 nM, one of the cassette compounds being the positive control diazepam. Equal volumes of matrix samples containing substances and blank dialysis buffer (Soerensen buffer at pH 7.4) were loaded into the opposite compartments of each well. The dialysis block was sealed and kept for 5 h at a temperature of 37 °C and 5% CO_2 environment in an incubator. After this time, equilibrium has been reached for most small molecule compounds with a molecular weight of <600. The seal was then removed and matrix and buffer from each dialysis was prepared for analysis by LC–MS/MS. All protein

binding determinations were performed in triplicate. The integrity of membranes was tested in the HT-Dialysis device by determining the unbound fraction values for the positive control diazepam in each well. At equilibrium, the unbound drug concentration in the biological matrix compartment of the equilibrium dialysis apparatus was the same as the concentration of the compound in the buffer compartment. Thus, the percentage unbound fraction (f_u) was calculated by determining the compound concentrations in the buffer and matrix compartments after dialysis as follows: $\%f_u = 100 \times$ buffer concentration after dialysis/matrix concentration after dialysis. The device recovery was checked by measuring the compound concentrations in the matrix before dialysis and calculating the percent recovery (mass balance). The recovery must be within 80 – 120% for data acceptance.

Pharmacokinetic analysis of LEI-515. Test compounds were formulated according to respective protocols either by dissolution (intravenous, i.v.) or in a glass potter until homogeneity was achieved (oral, p.o.). Formulations were injected i.v. using a 30 G needle in the lateral tail vein mice yielding a 10 mg/kg dose. For p.o. applications, animals were gavaged (yielding a 10 mg/kg dose). At the following time points blood was drawn into EDTA: 0.083, 0.25, 0.5, 1, 2, 4, 7 and 24 h. Three animals each were used for the i.v. and p.o. arm. Animals were distributed randomly over the time course and at each time point, a volume of 100 µl of blood was taken. Quantitative plasma measurement of the compound was performed by LC–MS/MS analysis. Pharmacokinetic analysis was conducted using Phoenix WinNonlin v.6.4 software using a noncompartmental approach consistent with the route of administration. For assessment of the exposure C_{max}, T_{max}, area under curve and bioavailability were determined from the plasma concentration profiles. Parameters (CL, Vss, $t_{1/2}$) were estimated using nominal sampling times relative to the start of each administration.

***In vivo* targets engagement studies of LEI-515 in mice**. Male C57BL/6J mice 8-10 weeks old at the time of dosing were maintained under a 12 h light/dark cycle and allowed free access to food and water. **LEI-515** was prepared fresh on the day of dosing in a DMSO/Kolliphore/5% mannitol in water (1/1/8, v/v) vehicle. Compounds were administered in a volume of 0.1 mL. Animals were administered single oral doses of

LEI-515 (5, 10 and 30 mg/kg) or vehicle. One hour after **LEI-515** administration, animals were killed by decapitation. The brains and lungs were collected and frozen in liquid nitrogen.

Lipid measurements in mouse brain and lung. Levels of 2-AG, AEA, AA and eicosanoids were measured by stable isotope dilution liquid chromatography/tandem mass spectrometry (LC-MS/MS) as described previously[40].

References

1. Senior, J. R.; Isselbacher, K. J. Demonstration of an intestinal monoglyceride lipase: an enzyme with a possible role in the intracellular completion of fat digestion. *The Journal of Clinical Investigation* **1963,** 42, 187-195.
2. Vaughan, M.; Berger, J. E.; Steinberg, D. Hormone-sensitive lipase and monoglyceride lipase activities in adipose tissue. *Journal of Biological Chemistry* **1964,** 239, 401-409.
3. Karlsson, M.; Contreras, J. A.; Hellman, U.; Tornqvist, H.; Holm, C. cDNA cloning, tissue distribution, and identification of the catalytic triad of monoglyceride lipase Evolutionary relationship to esterases, lysophospholipases, and haloperoxidases. *Journal of Biological Chemistry* **1997,** 272, 27218-27223.
4. Blankman, J. L.; Simon, G. M.; Cravatt, B. F. A comprehensive profile of brain enzymes that hydrolyze the endocannabinoid 2-arachidonoylglycerol. *Chemistry & biology* **2007,** 14, 1347-1356.
5. Baggelaar, M. P.; Maccarrone, M.; van der Stelt, M. 2-Arachidonoylglycerol: a signaling lipid with manifold actions in the brain. *Progress in lipid research* **2018,** 71, 1-17.
6. Sugiura, T.; Kodaka, T.; Nakane, S.; Miyashita, T.; Kondo, S.; Suhara, Y.; Takayama, H.; Waku, K.; Seki, C.; Baba, N. Evidence That the Cannabinoid CB1 Receptor Is a 2-Arachidonoylglycerol Receptor Structure-Activity Relationship of 2-Arachidonoylglycerol, Ether-linked Analogues, and Related Compounds. *Journal of Biological Chemistry* **1999,** 274, 2794-2801.
7. Sugiura, T.; Kondo, S.; Kishimoto, S.; Miyashita, T.; Nakane, S.; Kodaka, T.; Suhara, Y.; Takayama, H.; Waku, K. Evidence that 2-arachidonoylglycerol but not N-palmitoylethanolamine or anandamide is the physiological ligand for the cannabinoid CB2 receptor Comparison of the agonistic activities of various cannabinoid receptor ligands in HL-60 cells. *Journal of Biological Chemistry* **2000,** 275, 605-612.
8. Panikashvili, D.; Simeonidou, C.; Ben-Shabat, S.; Hanuš, L.; Breuer, A.; Mechoulam, R.; Shohami, E. An endogenous cannabinoid (2-AG) is neuroprotective after brain injury. *Nature* **2001,** 413, 527-531.
9. Kirkham, T. C.; Williams, C. M.; Fezza, F.; Marzo, V. D. Endocannabinoid levels in rat limbic forebrain and hypothalamus in relation to fasting, feeding and satiation: stimulation of eating by 2-arachidonoyl glycerol. *British journal of pharmacology* **2002,** 136, 550-557.
10. Yamaguchi, T.; Hagiwara, Y.; Tanaka, H.; Sugiura, T.; Waku, K.; Shoyama, Y.; Watanabe, S.; Yamamoto, T. Endogenous cannabinoid, 2-arachidonoylglycerol, attenuates naloxone-precipitated withdrawal signs in morphine-dependent mice. *Brain research* **2001,** 909, 121-126.
11. Fowler, C. J. Monoacylglycerol lipase–a target for drug development? *British journal of pharmacology* **2012,** 166, 1568-1585.
12. Aida, J.; Fushimi, M.; Kusumoto, T.; Sugiyama, H.; Arimura, N.; Ikeda, S.; Sasaki, M.; Sogabe, S.; Aoyama, K.; Koike, T. Design, Synthesis, and Evaluation of Piperazinyl Pyrrolidin-2-ones as a Novel Series of Reversible Monoacylglycerol Lipase Inhibitors. *J Med Chem* **2018,** 61, 9205-9217.
13. Butler, C. R.; Beck, E. M.; Harris, A.; Huang, Z.; McAllister, L. A.; Am Ende, C. W.; Fennell, K.; Foley, T. L.; Fonseca, K.; Hawrylik, S. J.; Johnson, D. S.; Knafels, J. D.; Mente, S.; Noell, G. S.; Pandit, J.; Phillips, T. B.; Piro, J. R.; Rogers, B. N.; Samad, T. A.; Wang, J.;

Wan, S.; Brodney, M. A. Azetidine and Piperidine Carbamates as Efficient, Covalent Inhibitors of Monoacylglycerol Lipase. *J Med Chem* **2017,** 60, 9860-9873.
14. Cisar, J. S.; Weber, O. D.; Clapper, J. R.; Blankman, J. L.; Henry, C. L.; Simon, G. M.; Alexander, J. P.; Jones, T. K.; Ezekowitz, R. A. B.; O'Neill, G. P.; Grice, C. A. Identification of ABX-1431, a Selective Inhibitor of Monoacylglycerol Lipase and Clinical Candidate for Treatment of Neurological Disorders. *J Med Chem* **2018,** 61, 9062-9084.
15. McAllister, L. A.; Butler, C. R.; Mente, S.; O'Neil, S. V.; Fonseca, K. R.; Piro, J. R.; Cianfrogna, J. A.; Foley, T. L.; Gilbert, A. M.; Harris, A. R.; Helal, C. J.; Johnson, D. S.; Montgomery, J. I.; Nason, D. M.; Noell, S.; Pandit, J.; Rogers, B. N.; Samad, T. A.; Shaffer, C. L.; da Silva, R. G.; Uccello, D. P.; Webb, D.; Brodney, M. A. Discovery of Trifluoromethyl Glycol Carbamates as Potent and Selective Covalent Monoacylglycerol Lipase (MAGL) Inhibitors for Treatment of Neuroinflammation. *J Med Chem* **2018,** 61, 3008-3026.
16. Cao, Z.; Mulvihill, M. M.; Mukhopadhyay, P.; Xu, H.; Erdélyi, K.; Hao, E.; Holovac, E.; Haskó, G.; Cravatt, B. F.; Nomura, D. K. Monoacylglycerol lipase controls endocannabinoid and eicosanoid signaling and hepatic injury in mice. *Gastroenterology* **2013,** 144, 808-817. e15.
17. Costola-de-Souza, C.; Ribeiro, A.; Ferraz-de-Paula, V.; Calefi, A. S.; Aloia, T. P. A.; Gimenes-Júnior, J. A.; de Almeida, V. I.; Pinheiro, M. L.; Palermo-Neto, J. Monoacylglycerol lipase (MAGL) inhibition attenuates acute lung injury in mice. *PloS one* **2013,** 8, e77706.
18. Nomura, D. K.; Morrison, B. E.; Blankman, J. L.; Long, J. Z.; Kinsey, S. G.; Marcondes, M. C. G.; Ward, A. M.; Hahn, Y. K.; Lichtman, A. H.; Conti, B. Endocannabinoid hydrolysis generates brain prostaglandins that promote neuroinflammation. *Science* **2011,** 334, 809-813.
19. Dajani, E.; Islam, K. Cardiovascular and gastrointestinal toxicity of selective cyclo-oxygenase-2 inhibitors in man. *J Physiol Pharmacol* **2008,** 59, 117-133.
20. Kinsey, S. G.; Nomura, D. K.; O'Neal, S. T.; Long, J. Z.; Mahadevan, A.; Cravatt, B. F.; Grider, J. R.; Lichtman, A. H. Inhibition of monoacylglycerol lipase attenuates nonsteroidal anti-inflammatory drug-induced gastric hemorrhages in mice. *Journal of Pharmacology and Experimental Therapeutics* **2011,** 338, 795-802.
21. Nomura, D. K.; Long, J. Z.; Niessen, S.; Hoover, H. S.; Ng, S. W.; Cravatt, B. F. Monoacylglycerol lipase regulates a fatty acid network that promotes cancer pathogenesis. *Cell* **2010,** 140, 49-61.
22. Nomura, D. K.; Lombardi, D. P.; Chang, J. W.; Niessen, S.; Ward, A. M.; Long, J. Z.; Hoover, H. H.; Cravatt, B. F. Monoacylglycerol lipase exerts dual control over endocannabinoid and fatty acid pathways to support prostate cancer. *Chem Biol* **2011,** 18, 846-56.
23. Schalk-Hihi, C.; Schubert, C.; Alexander, R.; Bayoumy, S.; Clemente, J. C.; Deckman, I.; DesJarlais, R. L.; Dzordzorme, K. C.; Flores, C. M.; Grasberger, B. Crystal structure of a soluble form of human monoglyceride lipase in complex with an inhibitor at 1.35 Å resolution. *Protein Science* **2011,** 20, 670-683.
24. Liu, Y.; Patricelli, M. P.; Cravatt, B. F. Activity-based protein profiling: the serine hydrolases. *Proceedings of the National Academy of Sciences* **1999,** 96, 14694-14699.
25. Niphakis, M. J.; Cravatt, B. F. Enzyme inhibitor discovery by activity-based protein profiling. *Annual review of biochemistry* **2014,** 83, 341-377.
26. Van Esbroeck, A. C.; Janssen, A. P.; Cognetta, A. B.; Ogasawara, D.; Shpak, G.; Van Der Kroeg, M.; Kantae, V.; Baggelaar, M. P.; De Vrij, F. M.; Deng, H. Activity-based protein profiling reveals off-target proteins of the FAAH inhibitor BIA 10-2474. *Science* **2017,** 356,

1084-1087.
27. Baggelaar, M. P.; Janssen, F. J.; van Esbroeck, A. C.; den Dulk, H.; Allarà, M.; Hoogendoorn, S.; McGuire, R.; Florea, B. I.; Meeuwenoord, N.; van den Elst, H. Development of an activity-based probe and in silico design reveal highly selective inhibitors for diacylglycerol lipase-α in brain. *Angewandte Chemie* **2013,** 125, 12303-12307.
28. Baggelaar, M. P.; Chameau, P. J.; Kantae, V.; Hummel, J.; Hsu, K.-L.; Janssen, F.; van der Wel, T.; Soethoudt, M.; Deng, H.; den Dulk, H. Highly selective, reversible inhibitor identified by comparative chemoproteomics modulates diacylglycerol lipase activity in neurons. *Journal of the American Chemical Society* **2015,** 137, 8851-8857.
29. Deng, H. *Chemical Tools to Modulate Endocannabinoid Biosynthesis*. Leiden Unversity: Leiden, 2017.
30. Ye, L.; Zhang, B.; Seviour, E. G.; Tao, K.-x.; Liu, X.-h.; Ling, Y.; Chen, J.-y.; Wang, G.-b. Monoacylglycerol lipase (MAGL) knockdown inhibits tumor cells growth in colorectal cancer. *Cancer letters* **2011,** 307, 6-17.
31. Pagano, E.; Borrelli, F.; Orlando, P.; Romano, B.; Monti, M.; Morbidelli, L.; Aviello, G.; Imperatore, R.; Capasso, R.; Piscitelli, F. Pharmacological inhibition of MAGL attenuates experimental colon carcinogenesis. *Pharmacological research* **2017,** 119, 227-236.
32. Kabsch, W. Xds. *Acta Crystallographica Section D: Biological Crystallography* **2010,** 66, 125-132.
33. McCoy, A. J.; Grosse-Kunstleve, R. W.; Adams, P. D.; Winn, M. D.; Storoni, L. C.; Read, R. J. Phaser crystallographic software. *Journal of applied crystallography* **2007,** 40, 658-674.
34. Winn, M. D.; Ballard, C. C.; Cowtan, K. D.; Dodson, E. J.; Emsley, P.; Evans, P. R.; Keegan, R. M.; Krissinel, E. B.; Leslie, A. G.; McCoy, A. Overview of the CCP4 suite and current developments. *Acta Crystallographica Section D: Biological Crystallography* **2011,** 67, 235-242.
35. Emsley, P.; Lohkamp, B.; Scott, W. G.; Cowtan, K. Features and development of Coot. *Acta Crystallographica Section D: Biological Crystallography* **2010,** 66, 486-501.
36. Baggelaar, M. P.; Chameau, P. J.; Kantae, V.; Hummel, J.; Hsu, K. L.; Janssen, F.; van der Wel, T.; Soethoudt, M.; Deng, H.; den Dulk, H.; Allarà, M.; Florea, B. I.; Di Marzo, V.; Wadman, W. J.; Kruse, C. G.; Overkleeft, H. S.; Hankemeier, T.; Werkman, T. R.; Cravatt, B. F.; van der Stelt, M. Highly Selective, Reversible Inhibitor Identified by Comparative Chemoproteomics Modulates Diacylglycerol Lipase Activity in Neurons. *J Am Chem Soc* **2015,** 137, 8851-7.
37. van Rooden, E. J.; Florea, B. I.; Deng, H.; Baggelaar, M. P.; van Esbroeck, A. C.; Zhou, J.; Overkleeft, H. S.; van der Stelt, M. Mapping in vivo target interaction profiles of covalent inhibitors using chemical proteomics with label-free quantification. *Nature protocols* **2018,** 13, 752.
38. Distler, U.; Kuharev, J.; Navarro, P.; Tenzer, S. Label-free quantification in ion mobility–enhanced data-independent acquisition proteomics. *Nature protocols* **2016,** 11, 795-812.
39. Mock, E. D.; Mustafa, M.; Gunduz-Cinar, O.; Cinar, R.; Petrie, G. N.; Kantae, V.; Di, X.; Ogasawara, D.; Varga, Z. V.; Paloczi, J. Discovery of a NAPE-PLD inhibitor that modulates emotional behavior in mice. *Nature Chemical Biology* **2020**, 1-9.

40. Mukhopadhyay, B.; Cinar, R.; Yin, S.; Liu, J.; Tam, J.; Godlewski, G.; Harvey-White, J.; Mordi, I.; Cravatt, B. F.; Lotersztajn, S. Hyperactivation of anandamide synthesis and regulation of cell-cycle progression via cannabinoid type 1 (CB1) receptors in the regenerating liver. *Proceedings of the National Academy of Sciences* **2011,** 108, 6323-6328.

Supplementary Information

Table S1. *In vitro* safety pharmacology profiling of LEI-515.

Targets	LEI-515 (µM)	% Inhibition of Control Specific Binding		
		1st	2nd	Mean
A_{2A}(h) (agonist radioligand)	10	8.1	15.2	11.7
α_{1A}(h) (antagonist radioligand)	10	7.3	-0.3	3.5
α_{2A}(h) (antagonist radioligand)	10	8.3	28.3	18.3
β_1(h) (agonist radioligand)	10	0.9	12.3	6.6
β_2(h) (antagonist radioligand)	10	25.6	28.0	26.8
BZD (central) (agonist radioligand)	10	-32.5	-13.0	-22.7
CB_1(h) (agonist radioligand)	10	18.7	25.8	22.3
CB_2(h) (agonist radioligand)	10	-8.9	-14.9	-11.9
CCK_1 (CCKA) (h) (agonist radioligand)	10	13.3	25.8	19.5
D_1(h) (antagonist radioligand)	10	2.1	10.2	6.2
D_{2S}(h) (agonist radioligand)	10	-3.4	7.7	2.2
ETA(h) (agonist radioligand)	10	-5.9	-10.1	-8.0
NMDA (antagonist radioligand)	10	11.1	1.6	6.3
H_1(h) (antagonist radioligand)	10	12.5	3.7	8.1
H_2(h) (antagonist radioligand)	10	-26.7	-25.3	-26.0
MAO-A (antagonist radioligand)	10	4.9	7.4	6.1
M_1(h) (antagonist radioligand)	10	-25.4	-33.6	-29.5
M_2 (h) (antagonist radioligand)	10	-6.8	-1.7	-4.2
M_3(h) (antagonist radioligand)	10	-24.6	-15.2	-19.9
N neuronal α4β2 (h) (agonist radioligand)	10	-7.8	-13.2	-10.5
δ (DOP) (h) (agonist radioligand)	10	53.0	43.7	48.3
kappa (h) (KOP) (agonist radioligand)	10	62.3	56.8	59.5
kappa (h) (KOP) (agonist radioligand)	1	12.8	30.6	21.7
µ (MOP) (h) (agonist radioligand)	10	25.6	15.2	20.4
5-HT_{1A}(h) (agonist radioligand)	10	8.8	12.4	10.6

5-HT_{1B} (h) (antagonist radioligand)	10	22.7	25.6	24.2
5-HT_{2A}(h) (agonist radioligand)	10	-5.5	-5.5	-5.5
5-HT_{2B}(h) (agonist radioligand)	10	30.7	24.4	27.6
5-HT_3(h) (antagonist radioligand)	10	-8.5	-7.8	-8.1
GR (h) (agonist radioligand)	10	29.5	30.8	30.2
AR(h) (agonist radioligand)	10	-1.1	-13.0	-7.0
V_{1a}(h) (agonist radioligand)	10	13.1	6.8	9.9
Ca^{2+} channel (L, dihydropyridine site) (antagonist radioligand)	10	58.2	50.6	54.4
Ca^{2+} channel (L, dihydropyridine site) (antagonist radioligand)	1	18.1	19.6	18.9
Potassium Channel hERG (human)- [3H] Dofetilide	10	8.5	3.0	5.8
KV channel (antagonist radioligand)	10	-1.2	-8.1	-4.7
Na^+ channel (site 2) (antagonist radioligand)	10	61.6	49.5	55.6
Na^+ channel (site 2) (antagonist radioligand)	1	12.6	-1.9	5.3
norepinephrine transporter(h) (antagonist radioligand)	10	24.9	25.7	25.3
dopamine transporter(h) (antagonist radioligand)	10	47.6	42.8	45.2
5-HT transporter (h) (antagonist radioligand)	10	10.3	-2.0	4.2
COX1(h)	10	13.4	-2.5	5.4
COX2(h)	10	20.3	-1.4	9.5
PDE3A (h)	10	-20.5	-33.8	-27.2
PDE4D2 (h)	10	-12.4	-20.9	-16.6
Lck kinase (h)	10	-9.2	-1.4	-5.3
acetylcholinesterase (h)	10	4.4	5.4	4.9

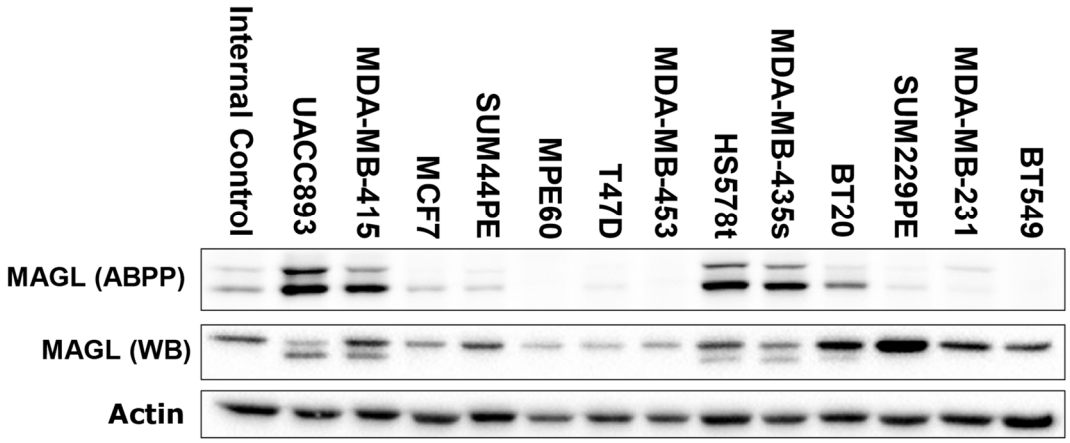

Figure S1. Profiling of MAGL activity and protein levels in a panel of 13 breast cancer cell lines.

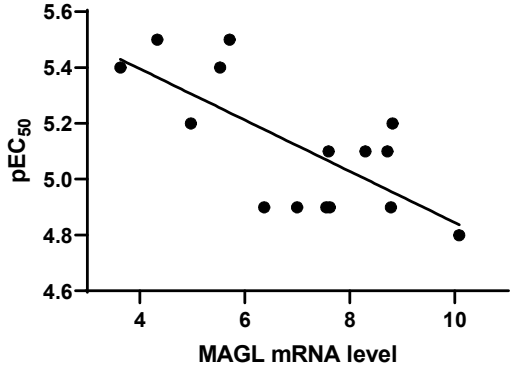

Figure S2. Plot of pEC_{50} of LEI-515 against MAGL mRNA levels in colorectal cancer cell lines.

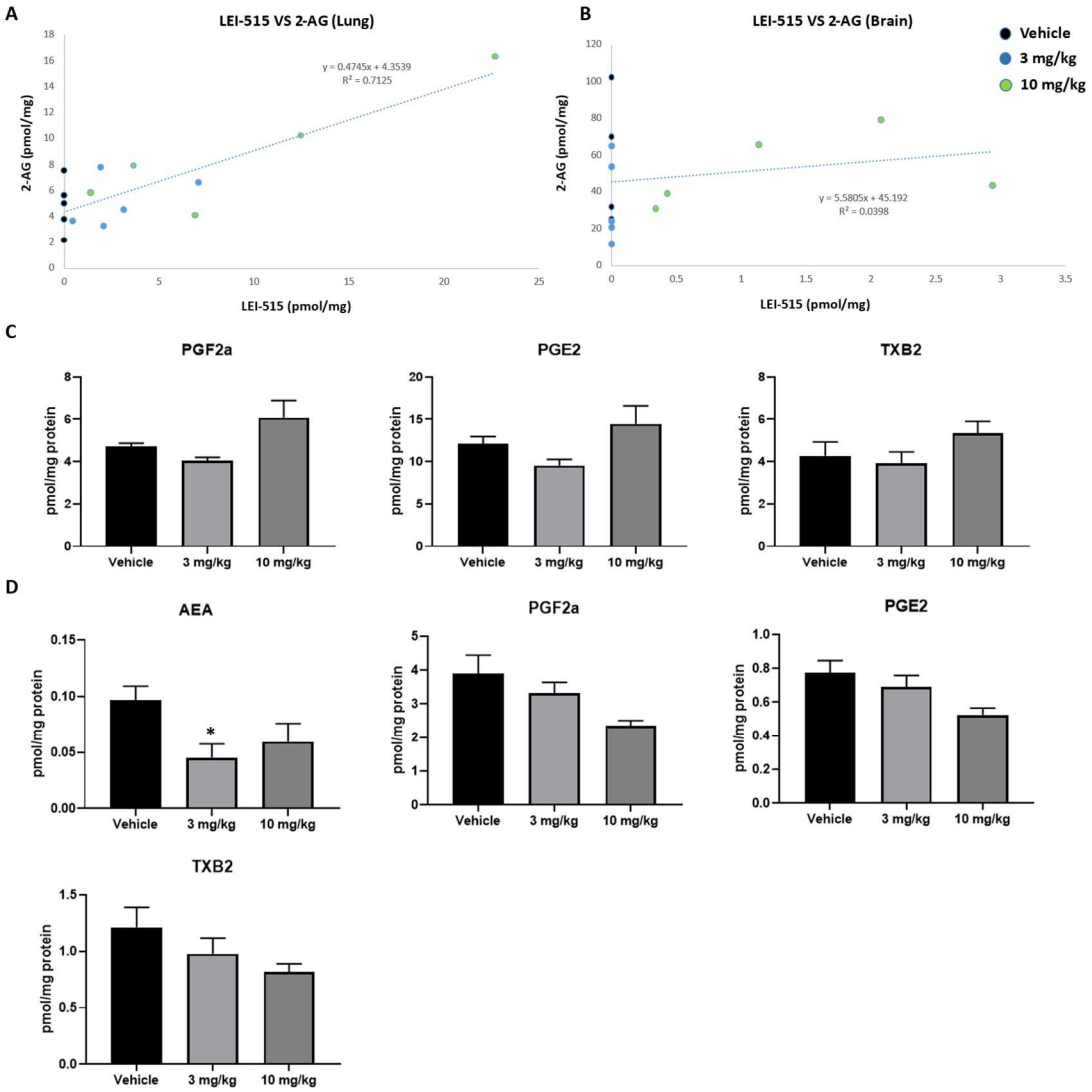

Figure S3. Plot of LEI-515 concentration versus 2-AG levels in the lung (A) and brain (B). (C) Absolute lipid levels of PGF2a, PGE2 and TXB2 in the lung (n = 5). (D) Absolute lipid levels of AEA, PGF2a, PGE2 and TXB2 in the brain (n = 5).